Proceedings of Computational Engineering Conference JSCES
Vol. 28, 2023 May

On the representation of discrete crack surfaces in crack phase-field model realized by finite cover method

(有限被覆法を用いた Crack phase-field モデルの離散き裂面の表現)

Jike Han [1)] Yuichi Shintaku [2)] Shuji Moriguchi [3)] and Kenjiro Terada [3)]

[1)]Department of Civil and Environmental Engineering, Tohoku University (E-mail:han.jike.s7@dc.tohoku.ac.jp)
[2)]Faculty of Engineering, Information and Systems, University of Tsukuba
[3)]International Research Institute of Disaster Science, Tohoku University

This study presents a diffusive-discrete crack transition scheme that can trace an actual crack path as closely as possible and stably update its explicit crack tip even in a large deformation regime. The crack initiation, propagation, and bifurcation processes are determined from an energy minimization problem with respect to the crack phase-field modeling. At the same time, the obtained diffusive crack path is replaced by a discrete representation by applying the finite cover method. The transition scheme is established within the dynamic fracture framework under the finite strain framework. Thus, a series of events from the crack initiation to the division of an original object into multiple portions and independent motions of divided portions can be simulated at once.

Key Words : *Crack phase-field, Finite cover method, Fracture, Finite strain*

1. INTRODUCTION

The crack phase-field model (CPFM) [1] is a promising approach for capturing arbitrary crack initiation, propagation, and bifurcation phenomena in materials. Recently, CPFMs have been combined with meshfree methods, such as XFEM, to realize the diffusive-discrete crack transition and to overcome shortcomings of the standard FEM, such as mesh distortion. While several studies [2–5], including authors' contribution, have been presented, the path has yet to be open to describe dynamic fracture.

In this context, this study enhances the diffusive-discrete crack transition scheme [5] to describe dynamic fracture under the finite strain framework. In the scheme, the crack initiation, propagation, and bifurcation processes are determined from an energy minimization problem with respect to the crack phase-field modeling. At the same time, the predicted path of a diffuse crack topology is replaced by a discrete representation by applying the FCM. Accordingly, the severely damaged region is no more continuous with respect to displacement, and independent motions of divided portions can be captured. After the formulation and the numerical algorithms are explained, representative numerical examples are presented to demonstrate the performance and capability of the developed scheme.

2. CPFM FOR DYNAMIC FRACTURE

Consider a continuum body under the finite strain framework. Then, the domain of the body and its boundary are defined as $\mathcal{B}_0 \subset \mathbb{R}^s$ & $\partial\mathcal{B}_0 \subset \mathbb{R}^s$ and $\mathcal{B}_t \subset \mathbb{R}^s$ & $\partial\mathcal{B}_t \subset \mathbb{R}^s$, which represent the initial and current configurations, respectively. Here, s denotes the dimensionality of the body. Also, the boundary conditions are imposed on the Neumann and Dirichlet boundaries, $\partial\mathcal{B}^{\mathrm{N}}$ and $\partial\mathcal{B}^{\mathrm{D}}$, respectively. To describe the deformation of the body, a mapping function $\boldsymbol{x} = \boldsymbol{\varphi}\left(\boldsymbol{X}, t\right)$ is introduced, which maps the points $\boldsymbol{X} \in \mathcal{B}_0$ onto points $\boldsymbol{x} \in \mathcal{B}_t$ at time $t \in \mathcal{T} = [0, T]$. Accordingly, $\boldsymbol{u} = \boldsymbol{x} - \boldsymbol{X}$ denotes the total displacement.

Meanwhile, the crack phase-field modeling is considered to describe the damage, for which a discrete crack Γ is numerically approximated as a diffusive crack $\Gamma_{l_{\mathrm{f}}}$ using a scalar variable d. Note that $d = 1$ is the fully broken state, whereas $d = 0$ is the sound state. In addition, the irreversibility condition of the damage evolution, i.e., $\dot{d} \geq 0$, is postulated.

Based on the first law of thermodynamics, the following energy conservation relation holds:

$$\mathcal{E} + \mathcal{K} + \mathcal{D} = \mathcal{P} \quad , \tag{1}$$

where

$$\begin{aligned}\mathcal{E} &= \int_{\mathcal{B}_0} \Psi \mathsf{dV} \\ &= \int_{\mathcal{B}_0} \left\{ \Psi^{\mathrm{e}}\left(\boldsymbol{F}, d\right) + \Psi^{\mathrm{f}}\left(d, \nabla d\right) \right\} \mathsf{dV},\end{aligned} \tag{2}$$

$$\mathcal{K} = \int_{\mathcal{B}_0} K \mathsf{dV} = \int_{\mathcal{B}_0} \frac{1}{2}\rho_0 \|\dot{\boldsymbol{u}}\|^2 \mathsf{dV} \quad , \tag{3}$$

$$\mathcal{D} = \int_{\mathcal{B}_0} D \mathsf{dV} = \int_{\mathcal{B}_0} \int_t \left(\boldsymbol{C} \cdot \dot{\boldsymbol{u}}\right) \cdot \dot{\boldsymbol{u}} \mathsf{dtdV} \quad , \tag{4}$$

and

$$\begin{aligned}\mathcal{P} &= \int_{\mathcal{B}_0} P_\mathrm{b}\mathsf{dV} + \int_{\partial\mathcal{B}_0} P_\mathrm{t}\mathsf{dA} \\ &= \int_{\mathcal{B}_0}\int_t \boldsymbol{B}\cdot\dot{\boldsymbol{u}}\mathsf{dtdV} + \int_{\partial\mathcal{B}_0}\int_t \boldsymbol{T}\cdot\dot{\boldsymbol{u}}\mathsf{dtdA}.\end{aligned} \tag{5}$$

Here, $\mathcal{E}$, $\mathcal{K}$, $\mathcal{D}$, and $\mathcal{P}$ denote the constitutive work potential, kinetic energy, dissipation energy, and external work. Also, Ψ, K, D, P_b, and P_t are the constitutive work density, kinetic energy density, dissipation energy density to due numerical damping, and external work densities of body and traction forces, respectively.

The constitutive work density Ψ is furthermore decomposed into the elastic strain energy density Ψ^e and crack generation energy density Ψ^f, whose specific forms are given as

$$\Psi^\mathrm{e} = \begin{cases} g(d)\left(\Psi^\mathrm{e}_{0,\mathrm{dev}} + \Psi^\mathrm{e}_{0,\mathrm{vol}}\right) + 0 & \text{for } J \geq 1 \\ g(d)\,\Psi^\mathrm{e}_{0,\mathrm{dev}} + \Psi^\mathrm{e}_{0,\mathrm{vol}} & \text{for } J < 1 \end{cases} \tag{6}$$

and

$$\Psi^\mathrm{f} = G_\mathrm{c}\gamma_{l_\mathrm{f}} = G_\mathrm{c}\frac{d^2 + l_\mathrm{f}\|\nabla d\|^2}{2l_\mathrm{f}}, \tag{7}$$

respectively. Here, $\boldsymbol{F} = \partial\boldsymbol{x}/\partial\boldsymbol{X}$ is the deformation gradient, and $J = \det[\boldsymbol{F}]$ denotes the determinant of the deformation gradient $\boldsymbol{F}$. Also, $g(d)$ is the degradation function to represent the deterioration of the material, and G_c & l_f are the fracture toughness and the crack length scale parameter, respectively. In addition, ∇ is a spatial gradient operator with respect to the initial configuration.

Meanwhile, the kinetic energy density K is computed from the mass density ρ_0 and the velocity vector $\dot{\boldsymbol{u}}$. Also, the dissipation energy density D is introduced as a numerical damping quantity for maintaining computational stability. In addition, the external work densities P_b & P_t are computed by the body force $\boldsymbol{B}$ and traction force $\boldsymbol{T}$, respectively.

Subsequently, the time derivative of Eq.(1) yields

$$\dot{\mathcal{E}} + \dot{\mathcal{K}} + \dot{\mathcal{D}} = \dot{\mathcal{P}} \quad , \tag{8}$$

and thus leads the following power balance equation:

$$\begin{aligned}&-\int_{\mathcal{B}_0}\left(\nabla\cdot\boldsymbol{P} + \boldsymbol{B} - \rho_0\ddot{\boldsymbol{u}} - \boldsymbol{C}\cdot\dot{\boldsymbol{u}}\right)\cdot\dot{\boldsymbol{u}}\mathsf{dV} \\ &-\int_{\mathcal{B}_0}\left(-\frac{\partial g(d)}{\partial d}\Psi^{\mathrm{e}+}_0 - \frac{G_\mathrm{c}}{l_\mathrm{f}}\left(d - l_\mathrm{f}^2\nabla^2 d\right)\right)\dot{d}\mathsf{dV} \\ &+\int_{\partial\mathcal{B}_0^\mathrm{N}}\left(\boldsymbol{P}\cdot\boldsymbol{N} - \bar{\boldsymbol{T}}\right)\cdot\dot{\boldsymbol{u}}\mathsf{dA} \\ &+\int_{\partial\mathcal{B}_0^\mathrm{D}}\left(\boldsymbol{P}\cdot\boldsymbol{N} - \boldsymbol{T}\right)\cdot\dot{\boldsymbol{u}}\mathsf{dA} \\ &+\int_{\partial\mathcal{B}_0} G_\mathrm{c}l_\mathrm{f}\nabla d\cdot\boldsymbol{N}\dot{d}\mathsf{dA} = 0\end{aligned} \quad . \tag{9}$$

Similarly, the first-order stability condition for any possible admissible variations $\{\delta\boldsymbol{u}, \delta d\}$ is given as

$$\begin{aligned}&-\int_{\mathcal{B}_0}\left(\nabla\cdot\boldsymbol{P} + \boldsymbol{B} - \rho_0\ddot{\boldsymbol{u}} - \boldsymbol{C}\cdot\dot{\boldsymbol{u}}\right)\cdot\delta\boldsymbol{u}\mathsf{dV} \\ &-\int_{\mathcal{B}_0}\left(-\frac{\partial g(d)}{\partial d}\Psi^{\mathrm{e}+}_0 - \frac{G_\mathrm{c}}{l_\mathrm{f}}\left(d - l_\mathrm{f}^2\nabla^2 d\right)\right)\delta d\mathsf{dV} \\ &+\int_{\partial\mathcal{B}_0^\mathrm{N}}\left(\boldsymbol{P}\cdot\boldsymbol{N} - \bar{\boldsymbol{T}}\right)\cdot\delta\boldsymbol{u}\mathsf{dA} \\ &+\int_{\partial\mathcal{B}_0} G_\mathrm{c}l_\mathrm{f}\nabla d\cdot\boldsymbol{N}\delta d\mathsf{dA} \geq 0\end{aligned} \quad . \tag{10}$$

From Eq.(9), Eq.(10), and the prescribed condition $\dot{d} \geq 0$, the governing equations of the displacement and damage fields are derived as follows:

$$\begin{aligned}\nabla\cdot\boldsymbol{P} + \boldsymbol{B} &= \rho_0\ddot{\boldsymbol{u}} + \boldsymbol{C}\cdot\dot{\boldsymbol{u}} && \text{in } \mathcal{B}_0 \\ \boldsymbol{P}\cdot\boldsymbol{N} &= \bar{\boldsymbol{T}} && \text{on } \partial\mathcal{B}_0^\mathrm{N} \\ \boldsymbol{u} &= \bar{\boldsymbol{u}} && \text{on } \partial\mathcal{B}_0^\mathrm{D}\end{aligned} \tag{11}$$

and

$$\left.\begin{array}{l} \underbrace{-\frac{\partial g(d)}{\partial d}\Psi^{\mathrm{e}+}_0 - \frac{G_\mathrm{c}}{l_\mathrm{f}}\left(d - l_\mathrm{f}^2\nabla^2 d\right)}_{\Phi^\mathrm{f}} \leq 0 \\ \dot{d} \geq 0 \\ \Phi^\mathrm{f}\dot{d} = 0 \end{array}\right\} \text{in } \mathcal{B}_0 \\ G_\mathrm{c}l_\mathrm{f}\nabla d\cdot\boldsymbol{N} = 0 \text{ on } \partial\mathcal{B}_0 \quad . \tag{12}$$

3. NUMERICAL ALGORITHM

Eq.(11) and Eq.(12) are spatially discretized by the FCM, and the Newmark method is employed to discretize time. Algorithm 1 presents the overview of the numerical algorithm employed in numerical simulations, which is an enhancement of the standard staggered iterative algorithm and realizes the transition from diffusive to discrete cracks; also refer to Han et al. [5]. Note that the algorithm enjoys the benefits of both the crack phase-field and the strong discontinuity of the FCM, which can reproduce the geometry of a discrete crack path that is propagated and even curved in a short time interval within the finite strain framework.

According to the algorithm, at each FC-based staggered iteration k, the damage and displacement fields are computed alternately. When both fields are determined, the configuration for computing the deformation gradient is updated. Subsequently, the norm of the staggered iterative residual $\boldsymbol{res}_{\mathrm{stag},k}$ is computed by

$$\begin{aligned}&\mathrm{norm}\left[\boldsymbol{res}_{\mathrm{stag},k}\right] \\ &\quad\text{with}\quad res^I_{\mathrm{stag},k} = \frac{\mathcal{E}^I_k + \mathcal{K}^I_k - \mathcal{E}^I_{k-1} - \mathcal{K}^I_{k-1}}{\mathcal{E}^I_k + \mathcal{K}^I_k}\end{aligned} \tag{13}$$

where the index I denotes the node number. If the value of this norm is smaller than the predefined threshold $\mathrm{TOL}_{\mathrm{st.}}$, two fields are considered converged at the current loading step, and a new displacement/force increment is imposed

ALGORITHM 1 FC-based staggered iterative algorithm for dynamic fracture.

```
(% At the time step $t_n$, $\boldsymbol{u}_{n,k=0} = \boldsymbol{u}_{n-1}$ and $d_{n,k=0} = d_{n-1}$ are known.)
Update the old velocity and acceleration for newmark method: $\dot{\boldsymbol{u}}_{n-1} = \dot{\boldsymbol{u}}_{n,k=0}$ and $\ddot{\boldsymbol{u}}_{n-1} = \ddot{\boldsymbol{u}}_{n,k=0}$
while norm $[\boldsymbol{res}_{stag,k}] > \mathrm{TOL}_{\mathrm{st.}}$ do
    $k = k + 1$ (% FC-based staggered iteration)
    NR loop: Compute the damage $\boldsymbol{d}_{n,k}$ with the fixed displacement $\boldsymbol{u}_{n,k-1}$
    NR loop: Compute the displacement $\boldsymbol{u}_{n,k}$ with the fixed damage $\boldsymbol{d}_{n,k}$
    Update configuration for computing deformation gradient: $\boldsymbol{X}_{n,k+1} = \boldsymbol{x}_{n,k}$
    Compute the staggered iterative residual by Eq.(13)
    if norm $[\boldsymbol{res}_{stag,k}] > \mathrm{TOL}_{\mathrm{st.}}$ then
        Check if the transition from diffusive to discrete cracks is needed; see Reference [5]
    end if
end while
```

for the next loading step. If not, the necessity of updating explicit crack tips is checked before going to the next FC-based staggered iteration $k + 1$.

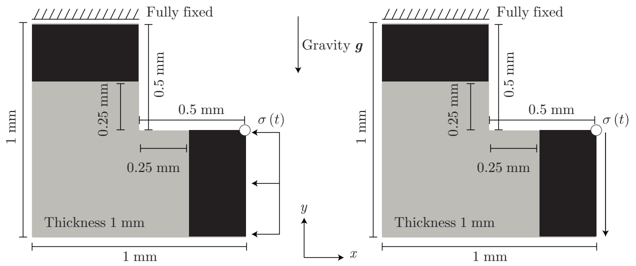

(a) Case lh **(b)** Case lv

Fig. 1: Geometry with boundary conditions.

Table 1: Material parameters.

Parameter		Value	Unit
Young's modulus	E	1.5×10^4	MPa
Poisson's ratio	ν	0.3	-
Density	ρ_0	1.0×10^3	kg/mm^3
Gravity	$\boldsymbol{g}$	$(0, -9.81, 0)$	mm/s^2
Fracture toughness	G_{c}	1.0	N/mm
Crack length scale parameter	l_{f}	0.015	mm
Pseudo-Lamé's constant	λ_{pse}	0.577	MPa
Pseudo-Lamé's constant	μ_{pse}	0.385	MPa

4. NUMERICAL SIMULATION

This example targets the impact failures of a L-shaped plate, whose geometry and boundary conditions are illustrated in Figure 1. As shown in the figure, the top edge is fully fixed, while the following sinusoidal pressure is horizontally or vertically applied to the right edge:

$$\sigma(t) = \begin{cases} \sigma_0 \sin\left(\dfrac{\pi}{0.005} t\right) & \text{if } 0 \leq t \leq 0.005 \text{ [s]} \\ 0 & \text{otherwise} \end{cases} \qquad (14)$$
$$\text{with} \quad \sigma_0 = 15 \text{ [MPa]}.$$

Also, the black-colored regions are assumed intact in simulations. This example aims to demonstrate a series of events of dynamic fracture that involves arbitrary crack initiation, propagation, bifurcation, division of the original object into multiple portions, and independent motions of divided portions. Material parameters are listed in Table 1, in which the gravity is assumed to be 0.1% of Earth's for visualization purposes. The cubic degradation function $g(d) = (s-2)(1-d)^3 + (3-s)(1-d)^2$ with $s = 0.1$ is used to represent the deterioration of the material.

The transition behavior of energy components and the snapshots of crack propagations are shown in Figure 2(a)-(d) and Figure 3, respectively. As shown in Figure 3, the crack initiation times and points, as well as propagation directions, differ with applied pressures: Case lh exhibits a single horizontal crack without a bifurcation, whereas Case lv exhibits a skew crack direction involving a bifurcation. In the meantime, the increases of initial energy are confirmed; see black-dashed lines in Figure 2(a) and Figure 2(c). These tendencies are due to the approximation capability of the finite covers. In fact, such ill-posed variations of energy are not observed before and after crack propagations; see Figure 2(b) and Figure 2(d).

On the other hand, the motions of two cases after divisions are shown in Figure 2(e) & (f) and Figure 4, respectively. Here, the values of displacement are taken from the white point at the top of the right edge, as shown in Figure 1. From Figure 2(e) & (f), the motions of the y direction exhibit free falls, while those of the x direction exhibit different tendencies in the two cases. To be specific, a constant velocity linear motion with small oscillations is confirmed for Case lh, while the motion of Case lv seems to be governed by rotation. In fact, Figure 4(b) indeed shows that the divided portion is free-falling and rotating. It is noted that the fall speed of Case lv is faster than that of Case hv because the pressure is applied horizontally and vertically.

Based on these numerical results, we confirm that the developed scheme is reasonable to simulate the series of events from the crack initiation to the independent motions of portions after crack propagation.

5. CONCLUSION

This study presents the transition scheme from diffusive to discrete crack topologies to describe dynamic fracture under the finite strain framework. The crack initi-

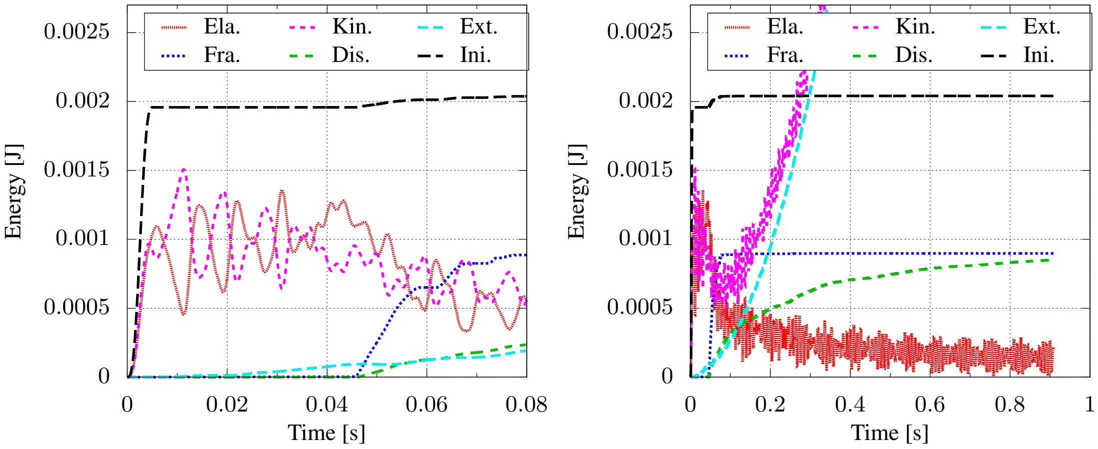

(a) Case lh ($0 \leq t \leq 0.08$ s)

(b) Case lh ($0 \leq t \leq 1$ s)

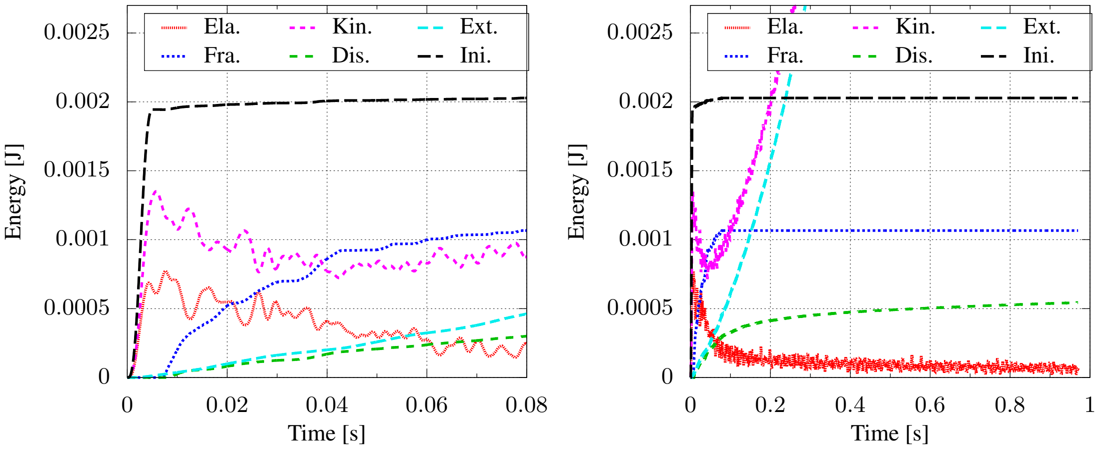

(c) Case lv ($0 \leq t \leq 0.08$ s)

(d) Case lv ($0 \leq t \leq 1$ s)

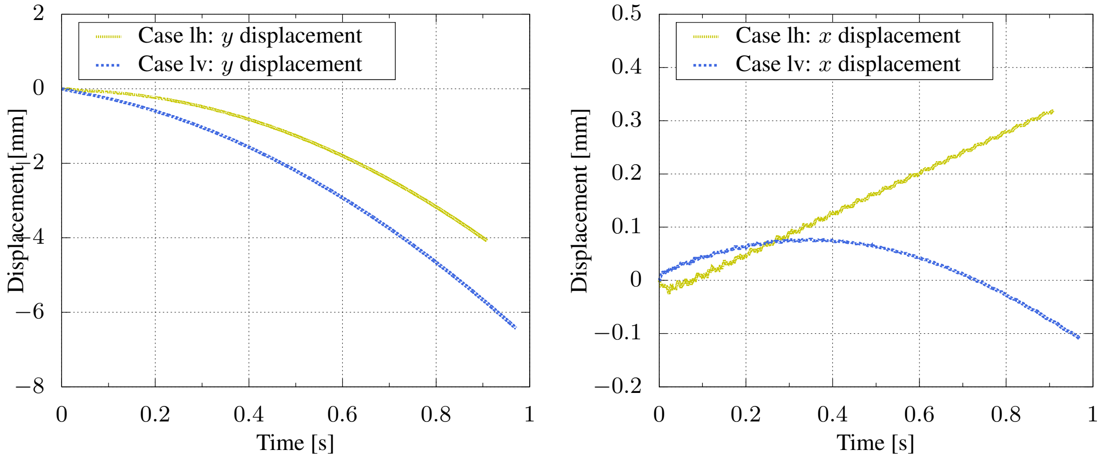

(e) y displacement

(f) x displacement

Fig. 2: Transition behavior of energy components and displacement-time relations. Ela: elastic strain energy; Fra: crack generation energy; Kin: kinetic energy; Dis: dissipation energy; Ext: external energy of body force; Ini: initial energy (Ela+Fra+Kin+Dis-Ext).

ation, propagation, and bifurcation processes are determined from an energy minimization problem, while the predicted crack path is explicitly represented by the FCM. Enjoying the feature of the scheme, a series of events of dynamic fracture involving arbitrary crack initiation, propagation, bifurcation, division of the portion, and independent motions of post-division, is successfully computed in one simulation.

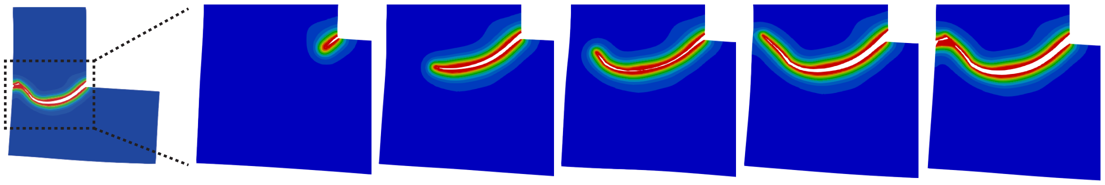

(a) Case lh

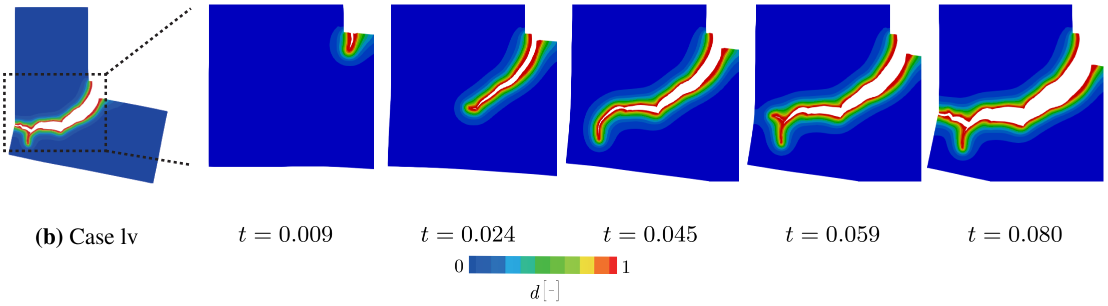

(b) Case lv

Fig. 3: Snapshots of crack propagations.

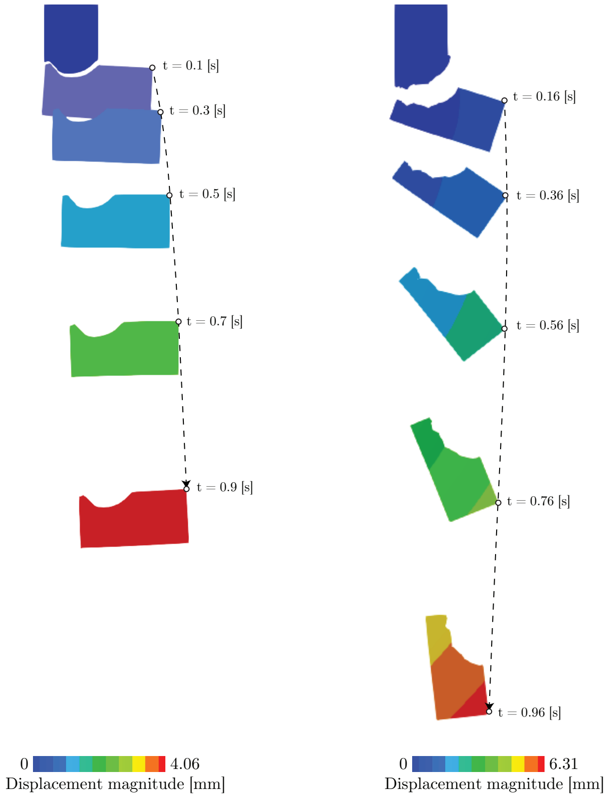

(a) Case lh (b) Case lv

Fig. 4: Trajectories of motions.

ACKNOWLEDGMENT This work was supported by JSPS KAKENHI Grant Number JP22J10932.

REFERENCES

[1] Miehe et al. *Int J Numer Methods Eng.* 2010; 83(10): 1273–1311. doi:10.1002/nme.2861

[2] Giovanardi et al. *Comput Methods Appl Mech Eng.* 2017; 320: 396–420. doi:10.1016/j.cma.2017.03.039

[3] Geelen et al. *Int J Numer Methods Eng.* 2018; 116(1): 1–20. doi:10.1002/nme.5911

[4] Hussein et al. *Comput Methods Appl Mech Eng.* 2020; 372: 113329. doi:10.1016/j.cma.2020.113329

[5] Han et al. *Int J Numer Methods Eng.* 2023; 124(6): 1405–1433. doi:10.1002/nme.7169